Scientia Iranica B (2017) 24(5), 2379–2386

Sharif University of Technology
Scientia Iranica
Transactions B: Mechanical Engineering
www.scientiairanica.com

Airflow patterns in a 3D model of the human acinus

M.A. Eslami Saray[a], M.S. Saidi[a*] and G. Ahmadi[b]

a. *Department of Mechanical Engineering, Sharif University of Technology, Tehran, Iran.*
b. *Department of Mechanical and Aeronautical Engineering, Clarkson University, New York, USA.*

Received 22 October 2014; received in revised form 31 July 2015; accepted 10 June 2017

KEYWORDS
Acinar region;
Alveoli;
Airflow pattern;
Computational fluid dynamics;
Dynamic mesh.

Abstract. Based on the recent photographs of microstructures of an acinus, a novel 3D computational model for airflow and particle transport and deposition was developed. To model the entire acinar region simultaneously, an approach was proposed to reduce the computational space. The airflow was solved using numerical simulations for the cases of expanding and contracting the acinus wall. The volume change of the lung was imposed based on the normal breathing condition with 15% volumetric expansion ratio. Since the entire acinar region was modeled, realistic pressure type boundary conditions were used and the use of earlier unrealistic boundary conditions was avoided. The simulation results showed that the flow patterns in an acinus with moving walls were significantly different from those in the rigid wall case. Furthermore, due to the asymmetric configuration, the flow patterns were not quite symmetric. It was shown that the ratio of alveolar flow to ductal flow rate controlled the dominant flow regime in each generation. Ratios below 0.005 led to recirculation regime, where flow separation occurred, while values above this threshold led to flows with radial streamlines. In summary, while the flow in the primary generations was characterized by the formation of recirculation regions in the alveoli, the terminal generations were characterized by radial streamlines, which moved towards the alveolar wall. Both flow regimes had substantial effects on particle deposition in the acinus.

1. Introduction

The complex nature of airflow in lung as a vital organ in human body has attracted the attention of applied mathematicians and biomedical engineers in addition to pulmonary physiologists. The main function of the lung is to exchange oxygen and carbon dioxide between the ambient air and capillaries surrounding the pulmonary passageways. An area of more recent concern has been the transport of the polluter into the airways and particle deposition on lung walls, which has many medical implications.

The first step to investigate the details of airflow in lung is to develop a realistic geometry and, then, develop a computational model for flow analysis. While the model geometry should be based on the anatomy of the lung, it should not be overly complex to allow for numerical solution with reasonable computational resources. Due to the intricate geometry of the lung and its differences among individuals, presenting one configuration for all human beings is impossible. Differences may stem from diameter and length in generations, or spatial angle of the branches in each bifurcation. As a result, the reported earlier studies are generally restricted to a particular region of the lung.

Human and mammalian lung resemble branching trees in which each generation (called mother) divides into two distinct branches (called daughters) consecutively for many generations ending in alveoli, which are the gas exchange units of the lung. The alveoli

*. *Corresponding author. Tel.: +98 21 66165558*
E-mail address: mssaidi@sharif.ir (M.S. Saidi)

doi: 10.24200/sci.2017.4304

may be divided into two regions: upper airways and lower airways. There is no gas exchange in the upper airways, but these conducting airways play a major role in the ventilation of lung. Geometric modeling of these airways is done using CT-scan data, human lung casts, or geometrical data proposed by primary physiological models [1-5].

Due to the small dimension of the lower airways, presenting a realistic model of this region is more challenging and needs advanced micro CT scan equipment for imaging. Considering morphologic data, lower airways begin from the sixteenth generation and last to the end of the lung. Although the total number of lung generations in each individual can vary from 18 to 30, on average, it is about 23 generations [6]. Unlike the conducting airways, which are similar to smooth-walled tubes, in the lower generations, alveoli are arranged as a foam-like sleeve on the surface of the peripheral airways. This region is also called alveolar region. Due to the existence of capillaries around the alveolar tissue, gas exchange occurs in this region. Recent studies estimate the mean number of alveoli about 480 million, with an average radius of about 100 μm [7].

Many geometric models for acinar region of human lung have been reported in the literature. Earlier models were limited to two dimensions and rather simple configuration, but over time, as more advanced imaging equipment became available, more realistic models were developed. To investigate the aerosol transport and deposition in the alveolar region of the human lung, Darquenne [8] has presented a 2D model of 6 consecutive generations of identical alveolated airways that were formed by dichotomous branching. The surface of the lumen was fully surrounded by alveoli in this model. Tippe and Tsuda [9] experimentally studied low Reynolds number flow patterns in acinar region. The geometry of their model consisted of a convective channel surrounded by a torus. The torus was an axisymmetric representation of a spherical alveolus, which was able to expand and contract, and captured the essential characteristics of the acinar structures. Harington et al. [10] used a model similar to that of Darquenne and Paiva [11], but considered the 3D geometry of each branch modeled as a cylindrical lumen surrounded by an annulus divided into discrete segments by axial and radial planes. These discrete segments represented the alveoli located on the main duct and entirely covered the duct. Harington et al. [10] also modeled a bifurcation and studied the particle deposition. Unlike other studies, which used Navier-Stokes equations or Monte Carlo method to study the acinar flow, Li and Kleinstreuer [12] employed the Lattice-Boltzmann method for numerical investigation of airflow patterns in this region. Using 2D alveolar geometries and imposing pressure inlet condition, they analyzed vortex propagation as well as the impact of alveolus expansion on airflow patterns, and pressure distributions for low inlet Reynolds number ranges.

Recently, Sznitman et al. [13] studied respiratory convective flows in the acinar region using an idealized 3D model based on Fung [14] description of the acinar ventilatory unit. Kumar et al. [15] considered different generations of an acinus individually to examine the acinar flow under imposed rhythmic breathing at varying Reynolds number. They attempted to highlight the role of geometries on the fluid exchange and the duct-cavity interactions.

The presented literature survey shows that the earlier papers investigated 2D or 3D models of a single generation or a bifurcation, and a model of the entire acinar region has not been developed yet. In the present paper, a 3D model of an entire acinus is proposed based on the respiratory dichotomous tree pattern. The model is based on the most recent geometry of a single alveolus and keeps the space-filling characteristic if possible. Unsteady simulation of airflow for the whole acinus, which consists of approximately 4600 alveoli, is desired. Numerical modeling and the novel idea, which makes it possible to simulate the fluid flow in this vast computational space, are presented in Section 3. Due to the comprehensive modeling, there is no need for unrealistic boundary conditions. All applied boundary conditions are described in Section 3.1. The magnitude and method of lung geometry change are other related issues in alveolar region modeling; thus, Section 3.2 is dedicated to the geometry change of the region. In order to check the accuracy of the proposed method, it is imposed and validated over smaller geometries in Section 3.3. Finally, results and the concluding remarks are made.

2. Model geometry

Fung [1988] recognized that alveoli were densely packed hollow polyhedral and suggested the truncated octahedron (or tetrakaidecahedron) for numerical simulation. The main reason for this selection is that the alveolar walls are predominantly hexagons and rectangles [14]. It also has the maximum ratio of surface area to volume among all space-filling polyhedrons. Using the truncated octahedron, one generation of the acinar region is modeled as shown in Figure 1. The geometry includes a main duct with three polyhedral models for the alveoli. Air inlet and outlet are on opposite sides of the main duct. The polyhedral sequence, representing alveoli, is placed around the main duct. There are three alveoli in the longitudinal direction and six in the radial direction; thus, there are 18 alveoli in each generation. Dimensions of all sides of each polyhedron are identical and the polyhedron is specified by only one characteristic length. This characteristic length is the

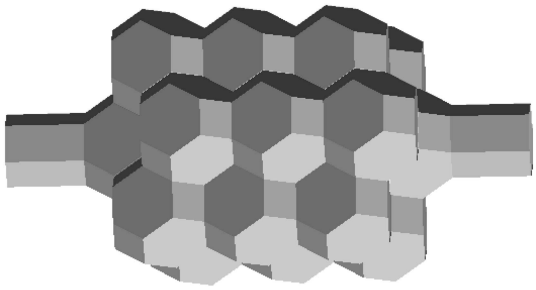

Figure 1. Geometric model for one generation of a human acinus.

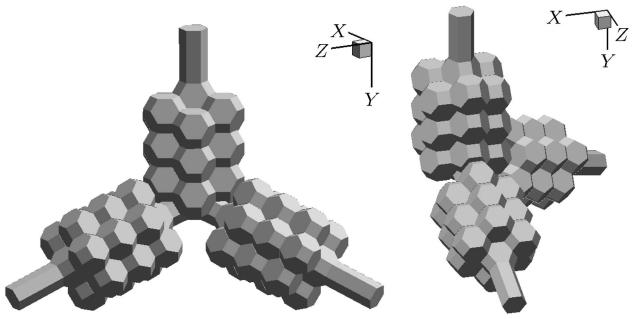

Figure 2. Geometric model for a bifurcation in the acinar region.

mean diameter of each generation, which was reported by Weible et al. [6].

By putting several generations together, a full model of acinar region is obtained. Earlier studies on bifurcations in the acinar region typically assumed that the two consecutive generations had the same diameter. As the diameters of the proximal and terminal generations of the acinus have significant differences, this assumption cannot be correct for the whole acinus model. The proposed model in this article has the ability to change the diameter in each bifurcation. The geometric model of a bifurcation is depicted in Figure 2. There is a small part between two consecutive generations, which has different diameters on each side. Thus, with the aid of this reduction part, the diameter of consecutive generations can decrease to desired proportions.

The full model of an acinus is obtained by extending the consecutive bifurcations as described above. This model would have about 2^8 generations, which is a vast computational space. In order to reduce the computational space, at the end of each generation, only one of the branches is continued and the other branch is truncated at the end of the reduction part. This way, the entire acinus can be represented by 9 main ducts along with their alveoli. The symmetry condition is applied at the truncated surfaces, which is described in Section 3. Figure 3 shows the proposed model for the entire acinar region. The boundaries where symmetry condition is applied are also illustrated. This model will be called "condensed model" in the text.

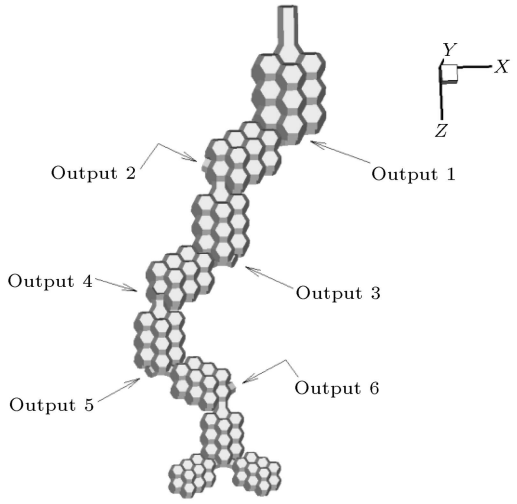

Figure 3. The condensed model representative of the entire acinus.

3. Numerical modeling

Due to the low airflow velocities in acinar region, the flow is in laminar regime. The airflow field is solved using the unsteady, incompressible Navier-Stokes equations with a commercial CFD code (Fluent 6.3). The continuity and Navier-Stokes equations in a moving mesh are expressed as:

$$\nabla.\mathbf{v} = 0, \tag{1}$$

$$\frac{\partial \mathbf{v}}{\partial t} + (\mathbf{v} - \mathbf{v}_g).\nabla\mathbf{v} = -\frac{1}{\rho}\nabla p + \nu\nabla^2\mathbf{v}, \tag{2}$$

where $\mathbf{v}$ is the fluid velocity vector field, $\mathbf{v}_g$ is the mesh velocity, p is the fluid pressure, and ρ and ν are the density and kinematic viscosity of air, respectively.

After grid and time step sensitivity studies, an unstructured mesh with a total number of 1,900,000 tetrahedral volume cells and a time step of 0.005 sec was used in the simulations. At each time step, a maximum residual of 10^{-3} was enforced for continuity and momentum balance equations. The Reynolds number, Re=$\mathbf{v}D/\nu$ was evaluated for each generation, where D was the effective diameter of the duct.

As noted above, modeling of the entire 8 generations of the acinar region is not feasible. Therefore, numerical solution of airflow in the condensed model should be evaluated in such a way that it correctly represents the flow patterns in the full acinar model. To achieve this goal, the symmetry boundary condition between continued branches and their counterparts, which are not continued (truncated branches), is imposed. This boundary condition is pressure type, similar to inlet/outlet boundary conditions. For this purpose, in each iteration, the magnitude of the total pressure on the continued Section is evaluated and this value is set on the truncated Section. Thus, the

magnitudes of the total pressures on both continued and truncated surfaces are identical.

3.1. Boundary conditions

Respiration and pulmonary ventilation occur due to the pressure difference between inside and outside of the lung. Therefore, in the study of the flow within the lung, all boundary conditions should be pressure type. In most studies, however, velocity or volumetric flow inlet boundary is used, which is not quite realistic. As the end of our model is closed, only one boundary condition is needed on the inlet/outlet boundary. Therefore, a constant pressure is imposed. The value of the gauge pressure on this boundary is set arbitrarily to zero.

Other boundary conditions are the magnitudes of velocities on walls. Acinar region is the main location for gas exchange in the lung and, hence, there is gas diffusion from the lung parenchyma to the blood capillaries. Due to the small amount of gas diffusion compared to the main airflow within the region, the gas penetration velocity on walls is ignored. Presence or absence of slip is determined by Knudsen number, which is defined as:

$$\mathrm{Kn} = \frac{2\lambda}{l}, \tag{3}$$

where l is the characteristic length and λ is the air mean free path. Magnitude of λ depends on the air temperature and pressure and is given as:

$$\lambda = \left(\frac{p_0}{p}\right)\left(\frac{T}{T_0}\right)\lambda_0, \tag{4}$$

where $\lambda_0 = 0.066\ \mu m$ is the mean free path at the standard conditions. Hence, the mean free path at the lung temperature is 0.06866 μm. The characteristic length of the problem is the main duct diameter; thus, Eq. [3] implies that the Knudsen number has the largest value at distal regions and terminal sacs. According to Weible et al. [6], the diameter of the last generation of acinus is 0.29 mm and the corresponding Knudsen number is 0.00046. Therefore, the Knudsen number even at terminal generation is quite small, the flow in the acinar region is in continuum regime, and no-slip boundary condition can be used. The last boundary condition is the symmetry condition on truncated branches, which is described above.

3.2. Wall motion

Air entry and exit during inspiration and expiration processes occur due to the volume change of the acinar region. Therefore, motion of the lung walls over time is the key mechanism for respiration. There are a number of models for volume change of acinar region [16]. These models typically depend on each individual condition such as rest, exercise, pulmonary health, or illness. The motion considered here is such that the model volume expands and contracts uniformly towards the volume centroid. All walls for ducts and/or alveoli remain parallel after the volume contraction or expansion and the topological shape of the region is invariant. That is, the scaling of length in all three Cartesian axes is the same.

Volume change of the acinar region plays the key role in the hydrodynamics of this region. The present model assumes 15% volumetric expansion ratio, which is identical to that proposed by Tippe and Tsuda [9]. Each ventilatory pattern consists of three characteristic parameters: [1] the tidal volume, [2] the ventilatory rate, and [3] the time relationship between Inhalation and Exhalation (I:E ratio). In normal breathing condition, which is considered for a healthy adult at rest, the tidal volume is about 7 to 9 mL/kg of ideal body weight and the breathing period is 3 sec with the I:E ratio of about 1:2 [16]. That is, in this respiratory pattern, 1 sec is for inhalation, 1 sec is for exhalation, and the remaining 1 sec pertains to the pause. As noted before, the wall motion is considered isotropic in all three axes of Cartesian coordinates. Due to the acinus geometry and its changes during the time, a dynamic mesh with spring based smoothing method is used. At each time step, the position of mesh nodes is evaluated using Eq. [5]:

$$\begin{cases} x_i = x_{i0}\left[1 + \beta\sin(\omega t)\right], & 0 < t < 2 \\ x_i = x_{i0}, & 2 \le t \le 3 \end{cases}, \tag{5}$$

where x_{i0} is the initial position of all mesh nodes; β is the expansion ratio in each direction, which is equal to 4.8%; and $\omega = \pi/2$ is the breathing frequency. The ratio of model volume to its primary volume (V/V_0) for two consecutive cycles is illustrated in Figure 4.

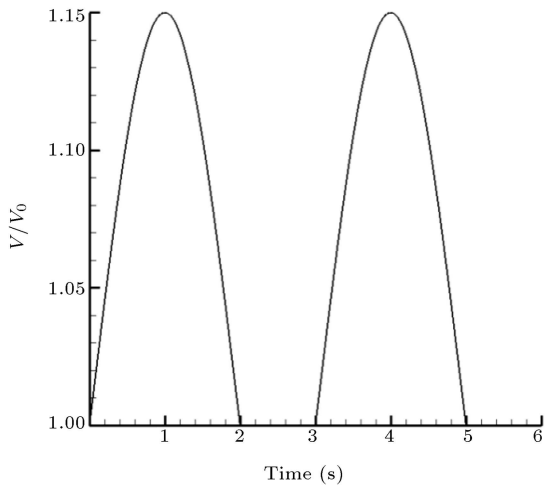

Figure 4. Ratio of model volume to its primary volume (V/V_0) during the respiration.

3.3. Validation

A full model of an acinus has not been investigated yet; thus, there is no detailed accurate data for model validation. The use of the truncated branches and the symmetry boundary condition for pressures used in the present simulations may cause uncertainties about the validity of the resulting airflow field. To validate the present approach, the flow in the alveolar region is solved for the three terminal generations. Due to the small computational space, in this case, it is possible to solve the flow in the entire configuration as well and, then, compare the results with the proposed method. Figure 5 shows both full and condensed models for the last three generations of the acinar region.

Boundary conditions and wall motion are identical to those described in Sections 3.1 and 3.2. The condensed model needs smaller time step and finer mesh than the full model. Figure 6(a) and (b), respectively, show the volumetric airflow rate at inlet and the first outlet/output (Output 1 in Figure 5(b)) as a function of the time of breathing. In the full model, the output is an interior surface while, in the condensed model, the outputs are outlets. It is seen that the volumetric flows of different sections of both models are almost identical, which indicates that the proposed approach is quite accurate. Table 1 is presented for more detailed comparison of the model prediction for volumetric flow at $t = 0.5$ sec. Results show the maximum difference of 0.3%.

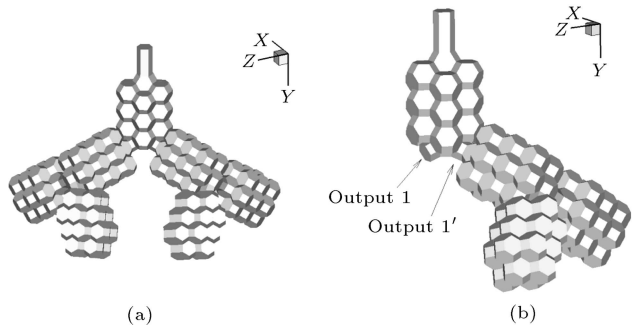

Figure 5. 3D models of the last three consecutive generations of the lung: (a) Full model, and (b) condensed model.

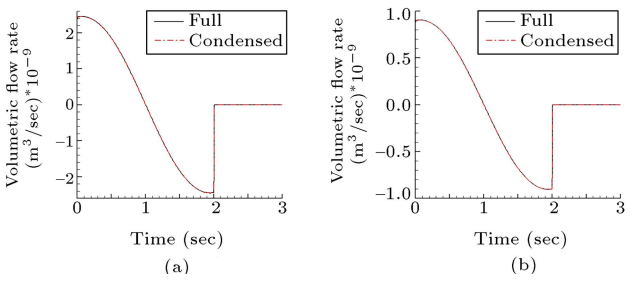

Figure 6. Volumetric flow rate for both models: (a) Inlet, and (b) first outlet.

Table 1. Exact values of volumetric flow rate at inlet and the first outlets of both models at $t = 0.5$ sec

Model	Flow at inlet $(m^3/sec)\times10^{-9}$	Flow at first outlet $(m^3/sec)\times10^{-10}$
Full	1.8518	6.8299
Condensed	1.8468	6.8124

4. Results and discussion

Figure 7 shows the normalized volumetric flow rate of the inlet/outlet boundary versus time. It is seen that the flow rate does not follow a completely sinusoidal pattern. The flow rate reaches its maximum value as the inhalation begins. Then, it decreases as the inhalation is continued and, at the end of inhalation, it becomes zero. As the exhalation begins, the air flows in a reverse direction and leaves the acinus. In earlier phase of exhalation, the flow rate is small and it reaches its maximum rate near the end of the exhalation cycle. Finally, at the end of exhalation, the volumetric flow again becomes zero, which persists until the end of pause time. The maximum volumetric flow rate (Q_{max}) is 5.77×10^{-8} m^3/sec.

Figure 8 shows the flow streamline at the mid-sections for different generations of an acinus. In the first generation Figure 8(a), the shear layer in the alveolar mouth openings causes the fluid to recirculate within the cavity. This shear layer is the result of the strong ductal flow, which is an order of magnitude larger than that in the alveoli. Due to the dichotomous structure of the tracheobronchial tree, the ductal flow rate decreases in the distal generations. Therefore, the shear layer and the recirculation become weaker in these generations. Figure 8(b) shows the streamlines for the fourth generation. It is seen that the stagnation saddle point approaches the proximal corner in each alveolus and decreases in size. Although the dominant

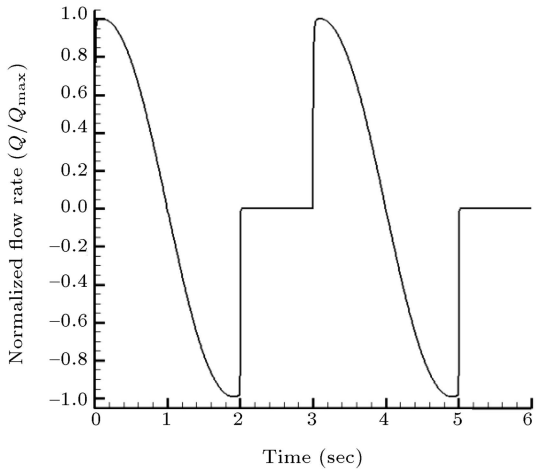

Figure 7. Normalized volumetric flow rate versus time.

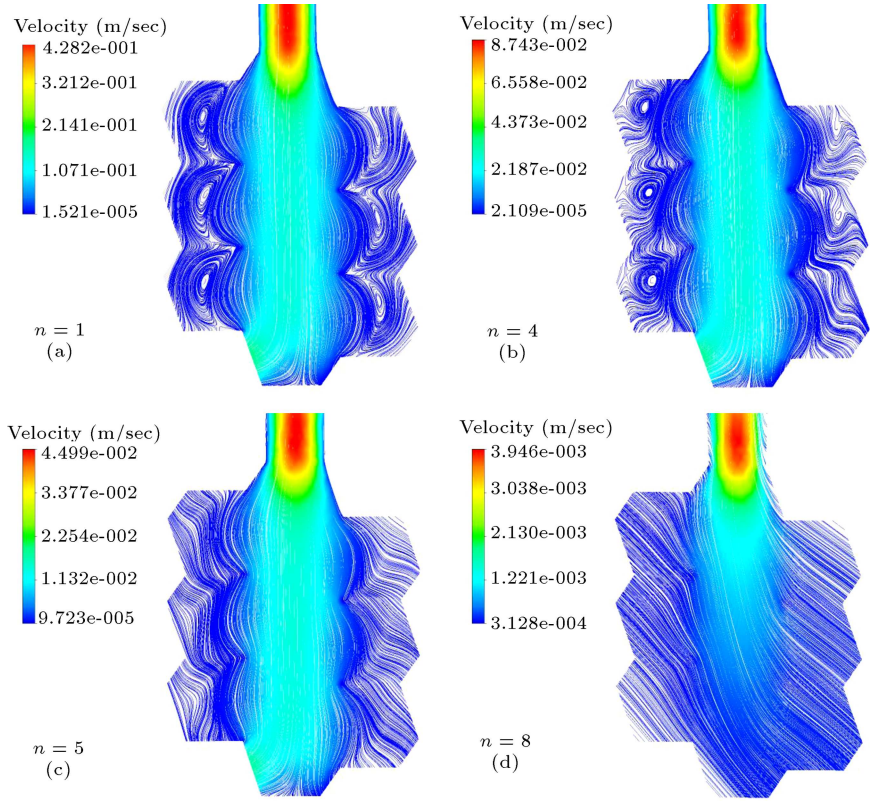

Figure 8. Streamline patterns at the mid-section of different generations: (a) First, (b) fourth, (c) fifth and (d) last.

pattern of this generation is the presence of the recirculation regions, there is also an imposed radial flow pattern. These radial streamlines are formed as a result of the geometry change. As the alveolar wall expands during inhalation, the alveoli play the role of flow sinks and stretch the streamlines towards their walls. This causes the formation of an entrainment region in the alveolar mouth opening, which itself results in a convective exchange between ductal flow and the flow in alveoli. It is also noteworthy that the asymmetry of the model causes the flow patterns in alveoli to be slightly different from one another. As the fluid gets further from inlet, the effect of expansion overcomes the shear layer and, finally, from the fifth generation Figure 8(c), the dominant flow pattern is the radial flow streamlines. In the last generation Figure 8(d), there is no open boundary and the entire ductal flow enters the alveoli. Therefore, no recirculation region forms.

If the walls are assumed to be rigid, there would be no radial flow streamline and, hence, no net alveolar flow rate. Figure 9 shows the streamlines for the rigid wall case. The streamlines are plotted for the first generation of an acinus for which the inlet boundary condition is a constant pressure and the outlet boundary condition is a sinusoidal flow rate. This figure shows that there is no radial flow streamline and all alveoli have regions with strong recirculation.

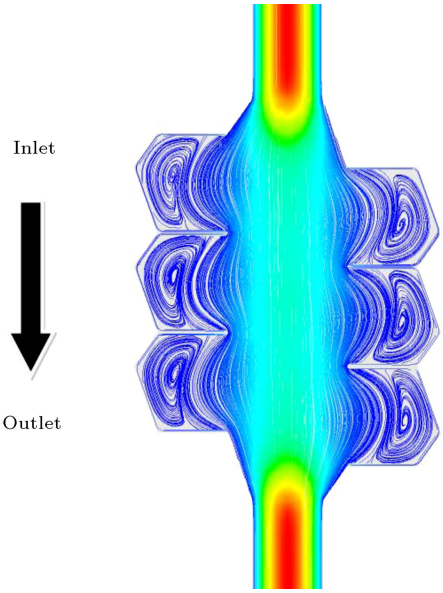

Figure 9. Streamlines for the rigid wall case.

Furthermore, the streamlines formed in the alveolar mouth opening separate the ductal flow from that in the alveoli. This flow pattern was also observed by Tippe and Tsuda [9].

With the above observations, it is concluded that the flow pattern in the alveolar region depends on two mechanisms. The first mechanism is the shear

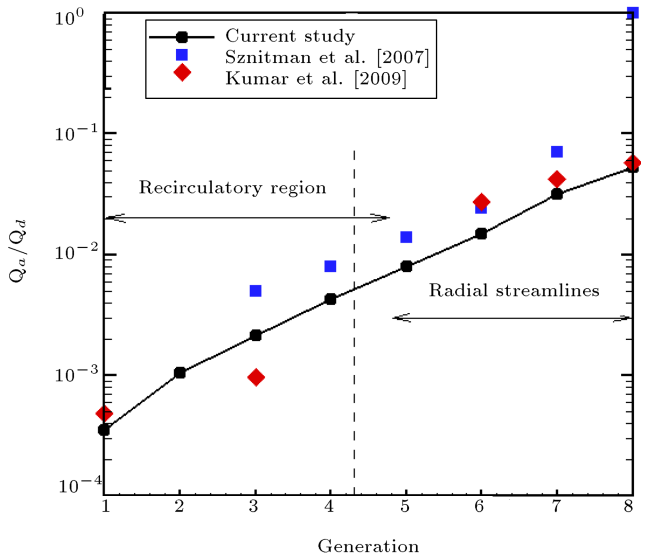

Figure 10. Alveolar to ductal flow ratio for different generations of an acinus.

layer, which is a function of the ductal flow rate, and the second one is the geometry change. In proximal generations, the ductal flow controls the flow pattern, while in distal generations, the effect of geometry change is more dominant. Hence, the alveolar to ductal flow rate ratio would be a good criterion to identify the dominant flow pattern in the alveolar region as was also reported earlier [13,15,17]. The alveolar flow rate is defined as the portion of the flow that enters the alveoli. Figure 10 compares the present model predictions for the alveolar to ductal flow rate ratio for different generations of the acinar region with the earlier works. It is estimated that the conversion of flow regime would happen between the fourth and the fifth generations. That is, the alveolar to ductal flow ratios less than 0.005 correspond to the recirculatory regime, while ratios greater than this threshold correspond to radial flow streamlines. It is also noteworthy that predictions of the present model are in reasonable agreement with the earlier report studies of [13,15,17]. The differences between present results and the earlier works perhaps originate from the variations in geometries and breathing conditions.

5. Conclusions

A novel 3D model of the acinus has been proposed based on the Fung's description of the acinar ventilatory unit and the dichotomous tree pattern. The details of the airflow have been evaluated under imposed rhythmic breathing, where the geometric shape of the model remains unchanged while its volume varies. Although the model has been truncated at each bifurcation, the airflow solution shows the flow patterns in the full model of an acinus. All boundary conditions have been pressure type, a constant pressure at inlet/outlet, and symmetry boundary condition at the truncated branches.

Despite the low Reynolds number flows in acinar region, complex airflow patterns have been observed. The simulation results show that airflow structures in proximal generations are roughly similar to those observed for a rigid wall model. Due to the strong ductal flow rate, separation may occur and the flow is characterized by the presence of recirculation regions, with only a small portion of the main flow entering the alveoli. In distal generations, in contrast, the relative importance of flow induced by the wall motion increases, which leads to a strong convective exchange between duct and the alveoli. This convective exchange was referred to as entrainment by Kumar et al. [15]. Hence, distal generations are mostly characterized by the radial flow streamlines. Both recirculating and radial flow streamlines significantly affect the particle deposition in the acinar region of the lung. The present simulation results also confirm that the alveolar to ductal flow ratio identifies the dominant flow regime. As the distal generations are approached, the alveolar to ductal flow ratio increases and the flow pattern changes from recirculating to radial. Simulation of the particle transport and deposition in the acinar region is left for a future study.

References

1. Liu, Y., So, R.M.C. and Zhang, C.H. "Modeling the bifurcating flow in a human lung airway", *Journal of Biomechanics*, **35**, pp. 465-473 (2002).
2. Rainhill, K., Freitas, R.K. and Schroder, W. "Numerical investigation of the three-dimensional flow in a human lung model", *Journal of Biomechanics*, **41**, pp. 2446-2457 (2008).
3. Calay, R.K., Kurujareon, J. and Hold, A.E. "Numerical simulation of respiratory flow patterns within human lung", *Respiratory Physiology and Neurobiology*, **130**, pp. 201-221 (2002).
4. Li, Z., Kleinstreuer, C. and Zhang, Z. "Simulation of airflow fields and microparticle deposition in realistic human lung airway models. Part I: Airflow patterns", *European Journal of Mechanics B/Fluids*, **26**, pp. 632-649 (2007).
5. Fresconi, F.E., Wexler, A.S. and Prasad, A.K. "Transport profiles in the conducting airways of the human lung", *International Journal of Heat and Mass Transfer*, **51**, pp. 5552-5561 (2008).
6. Weibel, E.R., Sapoval, B. and Filoche, M. "Design of peripheral airways for efficient gas exchange", *Respiratory Physiology and Neurobiology*, **148**, pp. 3-21 (2005).
7. Ochs, M., Nyengaard, J.R., Jung, A., Knudsen, L., Voigt, M., Wahlers, T., Richter, J. and Gundersen,

H.J.G. "The number of alveoli in the human lung", *The American Journal of Respiratory and Critical Care Medicine*, **169**, pp. 120-124 (2004).

8. Darquenne, C. "A realistic two–dimensional model of aerosol transport and deposition in the alveolar zone of the human lung", *Journal of Aerosol Science*, **32**, pp. 1161-1174 (2001).
9. Tippe, A. and Tsuda, A." Recirculating flow in an expanding alveolar model: Experimental evidence of flow-induced mixing of aerosol in the pulmonary acinus", *Journal of Aerosol Science*, **31**, pp. 979-986 (1999).
10. Harrington, L., Prisk, G.K. and Darquenne, C. "Importance of the bifurcation zone and branch orientation in simulated aerosol deposition in the alveolar zone of the human lung", *Journal of Aerosol Science*, **37**, pp. 37-62 (2006).
11. Darquenne, C., and Paiva, M. "Two–and three–dimensional simulations of aerosol transport and deposition in alveolar zone of the human lung", *Journal of Applied Physiology*, **80**, pp. 1401-1414 (1996).
12. Li, Z. and Kleinstreuer, C. "Airflow analysis in the alveolar region using the lattice-Boltzmann method", *Medical and Biological Engineering and Computing*, **49**, pp. 441-451 (2011).
13. Sznitman, J., Schmuki, S., Sutter, R., Tsuda, A. and Ro, T. "Sgen, CFD investigation of respiratory flows in a space-filling pulmonary acinus model", *Modelling in Medicine and Biology VII, WIT Transactions on Biomedicine and Health*, **12**, pp. 147-156 (2007).
14. Fung, Y.C. "A model of the lung structure and its validation", *Journal of Applied Physiology*, **64**, pp. 2132-2141 (1988).
15. Kumar, H., Tawhai, M.H., Hoffman, E.A. and Lin, C.L. "The effects of geometry on airflow in the acinar region of the human lung", *Journal of Biomechanics* **42**, pp. 1635-1642 (2009).
16. Jardins, T.D. "Cardiopulmonary Anatomy and Physiology: Essentials for Respiratory Care", Delmar, 4th Ed. (2002).
17. Henry, F.S., Butler, J.P. and Tsuda, A." Kinematically irreversible acinar flow: A departure from classical dispersive aerosol transport theories", *Journal of Applied Physiology*, **92**, pp. 835-845 (2002).

Biographies

Mohammad Ali Eslami Saray received his MSc degree in Mechanical Engineering from Sharif University of Technology (SUT). He received his BSc degree from Iran University of Science and Technology. His research interests are biofluids, modeling of particle transport and respiratory systems, and aerosol dynamics.

Mohammad Said Saidi is Professor of Mechanical Engineering at Sharif University of Technology. His research interests are modeling and numerical analysis of transport and deposition of aerosol particles, modeling and numerical analysis of biofluids, and respiratory system.

Goodarz Ahmadi is Professor of Mechanical and Aeronautical Engineering at Clarkson University. His research interests are aerosol transport, pollutant transport, and dispersion and turbulent flows of dense and dilute solid-gas or liquid mixture.